

Multi-study inference of regulatory networks for more accurate models of gene regulation

Dayanne M. Castro¹, Nicholas R. De Veaux², Emily R. Miraldi^{3,4}, Richard Bonneau^{1,2}

1 New York University, New York, NY 10003, USA

2 Center for Computational Biology, Flatiron Institute, New York, NY 10010, USA

3 Department of Pediatrics, University of Cincinnati College of Medicine, Cincinnati, OH 45229, USA

4 Divisions of Immunobiology & Biomedical Informatics, Cincinnati Children's Hospital, Cincinnati, OH 45229, USA

* rb133@nyu.edu

Abstract

Gene regulatory networks are composed of sub-networks that are often shared across biological processes, cell-types, and organisms. Leveraging multiple sources of information, such as publicly available gene expression datasets, could therefore be helpful when learning a network of interest. Integrating data across different studies, however, raises numerous technical concerns. Hence, a common approach in network inference, and broadly in genomics research, is to separately learn models from each dataset and combine the results. Individual models, however, often suffer from under-sampling, poor generalization and limited network recovery. In this study, we explore previous integration strategies, such as batch-correction and model ensembles, and introduce a new multitask learning approach for joint network inference across several datasets. Our method initially

estimates the activities of transcription factors, and subsequently, infers the relevant network topology. As regulatory interactions are context-dependent, we estimate model coefficients as a combination of both dataset-specific and conserved components. In addition, adaptive penalties may be used to favor models that include interactions derived from multiple sources of prior knowledge including orthogonal genomics experiments. We evaluate generalization and network recovery using examples from *Bacillus subtilis* and *Saccharomyces cerevisiae*, and show that sharing information across models improves network reconstruction. Finally, we demonstrate robustness to both false positives in the prior information and heterogeneity among datasets.

Introduction

Gene regulatory network inference aims at computationally deriving and ranking regulatory hypotheses on transcription factor-target gene interactions [1–3]. Often, these regulatory models are learned from gene expression measurements across a large number of samples. Strategies to obtain such data range from combining several publicly available datasets to generating large expression datasets from scratch [4–7]. Given decreasing costs of sequencing and the exponential growth in the availability of gene expression data in public databases [8,9], data integration across several studies becomes particularly promising for an increasing number of biological systems.

In theory, multi-study analyses provide a better representation of the underlying cellular regulatory network, possibly revealing insights that could not be uncovered from individual studies [6]. In practice, however, biological datasets are highly susceptible to batch effects [10], which are systematic sources of technical variation due to different reagents, machines, handlers etc. that complicate omics meta-analyses [11,12]. Although several methods to remove batch effects from expression data have been developed, they often rely on evenly distributed experimental designs across batches [13,14]. Batch-correction methods may deflate relevant biological variability or induce incorrect differences between

experimental groups when conditions are unbalanced across batches, which can significantly affect downstream analyses [15]. Therefore these batch effect removal methods are not applicable when integrating public data from multiple sources with widely differing experimental designs.

In network inference, an approach often taken to bypass batch effects is to learn models from each dataset separately and combine the resulting networks [16, 17]. Known as ensemble learning, this idea of synthesizing several weaker models into a stronger aggregate model is commonly used in machine learning to prevent overfitting and build more generalizable prediction models [18]. In several scenarios, ensemble learning avoids introducing additional artifacts and complexity that may be introduced by explicitly modeling batch effects. On the other hand, the relative sample size of each dataset is smaller when using ensemble methods, likely decreasing the ability of an algorithm to detect relevant interactions. As regulatory networks are highly context-dependent [19], for example, TF binding to several promoters is condition-specific [20], a drawback for both batch-correction and ensemble methods is that they produce a single network model to explain the data across datasets. Relevant dataset-specific interactions might not be recovered, or just difficult to tell apart using a single model.

Although it will not be the primary focus of this paper, most modern network inference algorithms integrate multiple data-types to derive prior or constraints on network structure. These priors/constraints have been shown to dramatically improve network model selection performance when combined with the state variables provided by expression data. In these methods [17, 21], priors or constraints on network structure (derived from multiple sources like known interactions, ATAC-seq, DHS, or ChIP-seq experiments [22–24]) are used to influence the penalty on adding model components, where edges in the prior are effectively penalized less. Here we describe a method that builds on that work (and similar work in other fields), but in addition we let model inference processes (each carried out using a separate data-set) influence each others model penalties, so that edges that agree across inference tasks are more likely to be uncovered [25–31]. Several previous works on this

front focused on enforcing similarity across models by penalizing differences on strength 46
and direction of regulatory interactions using a fusion penalty [25, 27, 28]. Because the 47
influence of regulators on the expression of targets may vary across datasets, possibly even 48
due to differences in measurement technologies, we look to induce similarity on network 49
structure (the choice of regulators) using a group-sparse penalty. Previous methods also 50
applied this type of penalty [26, 29, 31], however, they were not robust to differences in 51
relevant edges across datasets. 52

Here we propose a multitask learning (MTL) approach to exploit cross-dataset 53
commonalities while recognizing differences and is able to incorporate prior knowledge on 54
network structure if available [32, 33]. In this framework, information flow across datasets 55
leads the algorithm to prefer solutions that better generalize across domains, thus reducing 56
chances of overfitting and improving model predictive power [34]. Since biological datasets 57
are often under-sampled, we hypothesize that sharing information across models inferred 58
from multiple datasets using an explicit multitask learning framework will improve accuracy 59
of inferred network models in a variety of common experimental designs/settings. 60

In this paper, we explicitly show that joint inference significantly improves network 61
recovery using examples from two model organisms, *Bacillus subtilis* and *Saccharomyces* 62
cerevisiae. We show that models inferred for each dataset using our MTL approach (which 63
adaptively penalizes conserved and data-set-unique model components separately) are 64
vastly more accurate than models inferred separately using a single-task learning (STL) 65
approach. We also explore commonly used data integration strategies, and show that MTL 66
outperforms both batch-correction and ensemble approaches. In addition, we also 67
demonstrate that our method is robust to noise in the input prior information. Finally, we 68
look at conserved and dataset-specific inferred interactions, and show that our method can 69
leverage cross-dataset commonalities, while being robust to differences. 70

71

Results

72

Overview of network inference algorithm

73

To improve regulatory network inference from expression data, we developed a framework that leverages training signals across related expression datasets. For each gene, we assume that its regulators may overlap across conditions in related datasets, and thus we could increase our ability to uncover accurate regulatory interactions by inferring them jointly. Our method takes as input multiple expression datasets and priors on network structure, and then outputs regulatory hypotheses associated with a confidence score proportional to our belief that each prediction is true (Fig 1A). As previous studies [17,35–37], our method also includes an intermediate step that estimates transcription factor activities (TFA), and then, models gene expression as a function of those estimates (Fig 1B).

In our model, TFA represent a relative quantification of active protein that is inducing or repressing the transcription of its targets in a given sample, and is an attempt to abstract away unmeasured factors that influence TFA in a living cell [37–39], such as post-translational regulation [40], protein-protein interactions [41], and chromatin accessibility [42]. We estimate TFA from partial knowledge of the network topology (Fig 1C) [21,43–47] and gene expression data as previously proposed (Fig 1D) [17]. This is comparable to using a TF’s targets collectively as a reporter for its activity.

Next, we learn the dependencies between gene expression and TFA and score predicted interactions. In this step, our method departs from previous work, and we employ a multitask learning to learn regulatory models across datasets jointly, as opposed to single-task learning, where network inference is performed for each dataset independently (Fig 1E). As genes are known to be regulated by a small number of TFs [48], we can assume that these models are sparse, that is, they contain only a few nonzero entries [3]. We thus implement both approaches using sparsity-inducing penalties derived from the lasso [49]. Here the network model is represented as a matrix for each target gene (where

columns are data-sets/cell-types/studies and rows are potential regulators) with signed 98
entries corresponding to strength and type of regulation. 99

Importantly, our MTL approach decomposes this model coefficients matrix into a 100
dataset-specific component and a conserved component to enable us to penalize 101
dataset-unique and conserved interactions separately for each target gene [32]; this 102
separation captures differences in regulatory networks across datasets (Fig 2). Specifically, 103
we apply an l_1/l_∞ penalty to the one component to encourage similarity between network 104
models [50], and an l_1/l_1 penalty to the other to accommodate differences [32]. We also 105
incorporate prior knowledge by using adaptive weights when penalizing different 106
coefficients in the l_1/l_1 penalty [33]. Finally, we perform this step for several bootstraps of 107
the conditions in the expression and activities matrices, and calculate a confidence score for 108
each predicted interaction that represents both the stability across bootstraps and the 109
proportion of variance explained of the target expression dependent on each predictor. 110

Our method is readily available in an open-source package, *Inferelator-AMuSR* (**A**daptive 111
Multiple **S**parse **R**egression), enabling TF activity estimation and multi-source gene 112
regulatory network inference, ultimately facilitating mechanistic interpretations of gene 113
expression data to the Biology community. In addition, this method allows for adaptive 114
penalties to favor interactions with prior knowledge proportional to the user-defined belief 115
that interactions in the prior are true. Finally, our implementation also includes several 116
mechanisms that speed-up computations, making it scalable for the datasets here used, and 117
support for parallel computing across multiple nodes and cores in several computing 118
environments. 119

Model organisms, expression datasets, and priors 120

We validated our approach using two model organisms, a gram-positive bacteria, *B.* 121
subtilis, and an eukaryote, *S. cerevisiae*. Availability of validated TF-target regulatory 122
interactions, hereafter referred to as the gold-standard, make both organisms a good choice 123

for exploring inference methods (3040 interactions, connecting 153 TFs to 1822 target genes for *B. subtilis* [17, 46], 1198 interactions connecting 91 TFs to 842 targets for *S. cerevisiae* [51]). For *B. subtilis*, we use two expression datasets. The first one, *B. subtilis 1*, was collected for strain PY79 and contains multiple knockouts, competence and sporulation-inducing conditions, and chemical treatments (429 samples, 38 experimental designs with multiple time-series experiments) [17]. The second dataset, *B. subtilis 2*, was collected for strain BSB1 and contains several nutritional, and other environmental stresses, as well as competence and sporulation-inducing conditions (269 samples, and 104 conditions) [52]. For *S. cerevisiae*, we downloaded three expression datasets from the SPELL database [53]. *S. cerevisiae 1* is a compendium of steady-state chemostat cultures with several combinations of cultivation parameters (170 samples, 55 conditions) [54]. *S. cerevisiae 2* profiles two yeast strains (BY and RM) grown with two carbon sources, glucose and ethanol, in different concentrations (246 samples, and 109 conditions) [55]. Finally, *S. cerevisiae 3* with expression profiles following several mutations and chemical treatments (300 samples) [56]. Each dataset was collected using a different microarray platform. Cross-platform data aggregation is well known to cause of strong batch effects [10]. For each species, we considered the set of genes present across datasets.

In our inference framework, prior knowledge on network topology is essential to first estimate transcription factor activities and to then bias model selection towards interactions with prior information during the network inference stage of the algorithm. Therefore, to properly evaluate our method, it is necessary to gather prior interactions independent of the ones in the gold-standard. For *B. subtilis*, we adopt the previously used strategy of partitioning the initial gold-standard into two disjoint sets, a prior for use in network inference and a gold-standard to evaluate model quality [17]. For *S. cerevisiae*, on the other hand, we wanted to explore a more realistic scenario, where a gold-standard is often not available. In the absence of such information, we hypothesized that orthogonal high-throughput datasets would provide insight. Because the yeast gold-standard [51] was built as a combination of TF-binding (ChIP-seq, ChIP-ChIP) and TF knockout datasets

available in the YEASTRACT [47] and the SGD [57] databases, we propose to derive prior 152
knowledge from chromatin accessibility data [22,23] and TF binding sites [58] (as this is a 153
realistic and efficient genomic experimental design for non-model organisms). Open regions 154
in the genome can be scanned for transcription factor binding sites, which can provide an 155
indirect evidence of regulatory function [59]. We then assigned TFs to the closest upstream 156
gene, and built a prior matrix where entries represent the number of motifs for a particular 157
TF that was associated to a gene [60]. We obtained a list of regulators from the YeastMine 158
database [61], which we also used to sign entries in the prior: interactions for regulators 159
described as repressors were marked as negative. Because genome-wide measurements of 160
DNA accessibility can be obtained in a single experiment, using techniques that take 161
advantage of the sensitivity of nucleosome-free DNA to endonuclease digestion (DNase-seq) 162
or to Tn5 transposase insertion (ATAC-seq) [62], we expect this approach to be 163
generalizable to several biological systems. 164

Sharing information across network models via multitask learning 165 improves model accuracy 166

Using the above expression datasets and priors, we learn regulatory networks for each 167
organism employing both single-task and our multitask approaches. To provide an 168
intuition for cross-dataset transfer of knowledge, we compare confidence scores attributed 169
to a single gold-standard interaction using either STL or MTL for each organism. For *B.* 170
subtilis, we look at the interaction between the TF *sigD* and the gene *lytA* (Fig 3A). The 171
relationship between the *sigD* activity and *lytA* expression in the first dataset *B. subtilis 1* 172
is weaker than in *B. subtilis 2*. This is reflected in the predicted confidence scores, half as 173
strong for *B. subtilis 1* than for *B. subtilis 2*, when each dataset is used separately to learn 174
networks through STL. On the other hand, when we learn these networks in the MTL 175
framework, information flows from *B. subtilis 2* to *B. subtilis 1*, and we assign a high 176
confidence score to this interaction in both networks. Similarly, for *S. cerevisiae*, we look at 177
the interaction between the TF *Msn2* and the target gene *Hsp104* (Fig 3B). In this 178

particular case, we observe a stronger and easier-to-uncover relationship between *Msn2* 179
estimated activity and *Hsp104* expression as the size of the dataset increases. Using STL, 180
we assign a nonzero confidence score to this interaction for all datasets, although these are 181
much smaller than the scores attributed when networks are learned using MTL. 182

Following these examples, we examined changes in confidence scores attributed to all 183
interactions in the gold-standard in STL- and MTL-inferred networks (Fig 3C). Notably, 184
we see a high level of synergy between the *B. subtilis* datasets. Lots of interactions missed 185
by STL receive nonzero confidence scores through the MTL approach. For yeast, we 186
observe major gains of gold-standard interactions in particular for *S. cerevisiae 1*, which is 187
the dataset with the lowest number of samples. For datasets with larger sample size, *S.* 188
cerevisiae 2 and *S. cerevisiae 3*, we do not see similar synergy between datasets as in the *B.* 189
subtilis datasets, suggesting higher heterogeneity across the yeast datasets. 190

In order to evaluate the overall quality of the inferred networks, we use area under 191
precision-recall curves (AUPR) [16], widely used to quantify a classifier’s ability to 192
distinguish two classes and to rank predictions. Networks learned using MTL are 193
significantly more accurate than networks learned using the STL approach. For *B. subtilis* 194
(Fig 3D), we observe a 2-fold gain in AUPR, indicating significant complementarity between 195
the datasets. For *S. cerevisiae* (Fig 3E), we observe a clear increase in performance for 196
networks inferred for every dataset, indicating that our method is very robust to both data 197
heterogeneity and potential false edges derived from chromatin accessibility in the prior. 198

Benefits of multitask learning exceed those from batch-correction and 199 ensemble methods 200

Next, we asked whether the higher performance of the MTL framework could be achieved 201
by other commonly used data integration strategies, such as batch-correction and ensemble 202
methods. Ensemble methods include several algebraic combinations of predictions from 203
separate classifiers trained within a single-domain (sum, mean, maximum, minimum [63]). 204

To address this question, we evaluated networks inferred using all available data. First, we 205
combined regulatory models inferred for each dataset either through STL or MTL by 206
taking the maximum inferred confidence score for each interaction, generating two 207
networks hereafter called STL-C and MTL-C. Although taking the average is more 208
commonly done (in particular, when multiple algorithms are applied to the same dataset, 209
which is not the case here) [16], this would emphasize particularly the commonalities across 210
datasets. In addition, the motivation to use an MTL framework is to increase statistical 211
power, while maintaining separate models for each dataset, hopefully improving 212
interpretability. For each organism, we also merged all datasets into one, and applied 213
ComBat for batch-correction [64], because of its perceived higher performance [65]. We 214
then learn network models from these larger batch-corrected datasets, STL-BC. Both for *B.* 215
subtilis (Fig 4A) and *S. cerevisiae* (Fig 4B), the MTL-C networks significantly outperform 216
the STL-C and STL-BC networks, indicating that cross-dataset information sharing during 217
modelling is a better approach to integrate datasets from different domains. Interestingly, 218
the STL-BC networks' increase in performance, as compared to STL networks in Fig 3, was 219
more pronounced in yeast than in *B. subtilis*. We speculate that the higher overlap 220
between the conditions in the two *B. subtilis* datasets led to lower additional information 221
when merging them together. Moreover, batch-correcting in this scenario may have 222
decreased dataset-specific variability. For yeast, on the other hand, conditions were very 223
different across datasets, and much new information is gained by merging them into one. 224
However, because of this very fact, it is likely that incorrect relationships between genes 225
were induced as an artifact, possibly confounding the inference. 226

Our method is robust to increasing prior weights and noise in prior 227

Because genes are frequently co-regulated, and biological networks are redundant and 228
robust to perturbations, spurious correlations between transcription factors and genes are 229
highly prevalent in gene expression data [66,67]. To help discriminate true from false 230
interactions, it is essential to incorporate prior information to bias model selection towards 231

interactions with prior knowledge. Indeed, incorporating prior knowledge has been shown 232
shown to increase accuracy of inferred models in several studies [3, 21, 68]. 233

For example, suppose that two regulators present highly correlated activities, but regulate 234
different sets of genes. A regression-based model would be unable to differentiate between 235
them, and only other sources of information, such as binding evidence nearby a target gene, 236
could help selecting one predictor over the other in a principled way. Thus, we provide an 237
option to integrate prior knowledge to our MTL approach in the model selection step by 238
allowing the user to input a “prior weight”. This weight is used to increase presence of prior 239
interactions to the final model, and should be proportional to the quality of the input prior. 240

Sources of prior information for the two model organisms used in this study are 241
fundamentally different. The *B. subtilis* prior is high-quality, derived from small-scale 242
experiments, whereas the *S. cerevisiae* prior is noisier, likely with both high false-positive 243
and false-negative rates, derived from high-throughput chromatin accessibility experiments 244
and TF binding motifs. To understand differences in prior influences for the same 245
organism, we also include the yeast gold-standard as a possible source of prior in this 246
analysis. The number of TFs per target gene in the *B. subtilis* (Fig 5A) and the *S.* 247
cerevisiae (Fig 5B) gold-standards (GS) is hardly ever greater than 2, with median of 1, 248
whereas for the chromatin accessibility-derived priors (ATAC) for *S. cerevisiae*, the median 249
is 11 (Fig 5C). A large number of regulators per gene likely indicates a high false-positive 250
rate in the yeast ATAC prior. Given the differences in prior quality, we test the sensitivity 251
of our method to the prior weight parameter. We applied increasing prior weight, and 252
measured how the confidence scores attributed to prior interactions was affected (Fig 5C) 253
for the three described above source of priors. Interestingly, the confidence scores 254
distributions show dependencies on both the prior quality and the prior weights. When the 255
gold-standard interactions for *B. subtilis* and *S. cerevisiae* are used as prior knowledge, 256
they receive significantly higher scores than interactions in the *S. cerevisiae* chromatin 257
accessibility-derived prior, which is proportional to our belief on the quality of the input 258
prior information. Importantly, even when we set the prior weight value to a very high 259

value, such as 10, interactions in the ATAC prior are not pushed to very high confidence 260
scores, suggesting that our method is robust to the presence of false interactions in the 261
prior. 262

Joint network inference is robust to dataset heterogeneity 263

Because multitask learning approaches are inclined to return models that are more similar 264
to each other, we sought to understand how heterogeneity among datasets affected the 265
inferred networks. Specifically, we quantified the overlap between the networks learned for 266
each dataset for *B. subtilis* and yeast. That is, the number of edges that are unique or 267
shared across networks inferred for each dataset (Fig 6). In this analysis, we consider valid 268
only predictions within a 0.5 precision cut-off, calculated using only TFs and genes present 269
in the gold-standard. Since the *B. subtilis* datasets share more conditions than the yeast 270
datasets, we hypothesized that the *B. subtilis* networks would have a higher overlap than 271
the yeast networks. As expected, we observe that about 50% of the total edges are shared 272
among two *B. subtilis* networks (Fig 6A), whereas for yeast only about 31% (Fig 6B) and 273
35% (Fig 6C), using gold-standard and chromatin accessibility-derived priors respectively, 274
of the total number of edges is shared by at least two of the three inferred networks. 275
Therefore, our approach for joint inference is robust to cross-dataset influences, preserving 276
relative uniqueness when datasets are more heterogeneous. 277

Discussion 278

In this study, we presented a multitask learning approach for joint inference of gene 279
regulatory networks across multiple expression datasets that improves performance and 280
biological interpretation by factoring network models derived from multiple datasets into 281
conserved and dataset-specific components. Our approach is designed to leverage 282
cross-dataset commonalities while preserving relevant differences. While other multitask 283

methods for network inference penalize for differences in model coefficients across 284
datasets [25–28, 30], our method leverages shared underlying topology rather than the 285
influence of TFs on targets. We expect this method to be more robust, because, in living 286
cells, a TF’s influence on a gene’s expression can change in different conditions. In 287
addition, previous methods either deal with dataset-specific interactions [25], or apply 288
proper sparsity inducing regularization penalties [26–30]. Our approach, on the other hand, 289
addresses both concerns. Finally, we implemented an additional feature to allow for 290
incorporation of prior knowledge on network topology in the model selection step. 291

Using two different model organisms, *B. subtilis* and *S. cerevisiae*, we show that joint 292
inference results in accurate network models. We also show that multitask learning leads to 293
more accurate models than other data integration strategies, such as batch-correction and 294
combining fitted models. Generally, the benefits of multitask learning are more obvious 295
when task overlap is high and datasets are slightly under-sampled [34]. Our results support 296
this principle, as the overall performance increase of multitask network inference for *B.* 297
subtilis is more pronounced than for *S. cerevisiae*, which datasets sample more 298
heterogeneous conditions. Therefore, to benefit from this approach, defining input datasets 299
that share underlying regulatory mechanisms is essential and user-defined. 300

A key question here, that requires future work, is the partitioning of data into separate 301
datasets. Here we use the boundaries afforded by previous study designs: we use data from 302
two platforms and two strains for *B. subtilis* (a fairly natural boundary) and the separation 303
between studies by different groups (again using different technologies) in yeast. We choose 304
these partitions to illustrate robustness to the more common sources of batch effect in 305
meta-analysis. In the future, we expect that multitask methods in this domain will 306
integrate dataset partition estimation (which data go in which bucket) with network 307
inference. Such methods would ideally be able to estimate task similarity, taking into 308
account principles of regulatory biology, and apply a weighted approach to information 309
sharing. In addition, a key avenue for future work will be to adapt this method to 310
multi-species studies. Examples multitask settings of high biological and biomedical 311

interest include joint inferences that include model system and organisms of primary 312
interest (for example data-set that include mouse and human data collected for similar cell 313
types in similar conditions). These results (and previous work on many fronts [7, 25, 69]) 314
suggest that this method would perform well in this setting. Nevertheless, because of the 315
increasing practice of data sharing in Biology, we speculate that cross-study inference 316
methods will be largely valuable in the near future, being able to learn more robust and 317
generalizable hypotheses and concepts. Although we present this method as an alternative 318
to batch correction, we should point out that there are many uses to batch correction that 319
fall outside of the scope of network inference, and our results do not lessen the applicability 320
of batch correction methods to these many tasks. There is still great value in properly 321
balancing experimental designs when possible to allow for the estimation of specific gene- 322
and condition-wise batch effects. Experiments where we interact MTL learning with 323
properly balanced designs and quality batch correction are not provided here, but would be 324
superior. Thus, the results here should be strictly interpreted in the context of network 325
inference, pathway inference, and modeling interactions. 326

Methods 327

Expression data selection, preprocessing and batch-correction 328

For *B. subtilis*, we downloaded normalized expression datasets from the previously 329
published network study by Arrieta-Ortiz *et al* [17]. Both datasets are available at GEO, 330
B. subtilis 1 with accession number GSE67023 [17] and *B. subtilis 2* with accession number 331
GSE27219 [52]. For yeast, we downloaded expression datasets from the SPELL database, 332
where hundreds of re-processed gene expression data is available for this organism. In 333
particular, we selected three datasets from separate studies based on the number of 334
samples, within-dataset condition diversity, and cross-dataset condition overlap (such as 335
nutrient-limited stress). *S. cerevisiae 1* and *S. cerevisiae 2* are also available at GEO at 336

accession numbers GSE11452 [54] and GSE9376 [55]. *S. cerevisiae* 3 does not have a GEO 337
accession number, and was collected in a custom spotted microarray [56]. For network 338
inference, we only kept genes present in all datasets, resulting in 3780 and 4614 genes for *B.* 339
subtilis and for yeast respectively. In order to join merge, for comparison, we consider each 340
dataset to be a separate batch, since they were generated in different labs as part of 341
separate studies, and applied ComBat for batch-correction using default parameters and no 342
reference to experimental designs [64]. 343

Building priors from chromatin accessibility 344

ATAC-seq data download, processing, and peak calling 345

We downloaded chromatin accessibility data *S. cerevisiae* from the European Nucleotide 346
Archive (PRJNA276699) [70, 71]. Reads were mapped to the sacCer3 genome (iGenomes, 347
UCSC) using bowtie2 [72] with the options `-very-sensitive -maxins 2000`. Reads with low 348
mapping quality ($\text{MAPQ} < 30$), or that mapped to mitochondrial DNA were removed. 349
Duplicates were removed using Picard. Reads mapping the forward strand were offset by 350
`+4 bp`, and reads mapping to the reverse strand `-4 bp`. Accessible regions were called using 351
MACS2 [73] with the options `-qvalue 0.01 -gsize 12100000 -nomodel -shift 20 -extsize 40`. 352
We defined the union of peaks called in any the ATAC-seq samples as the set of putative 353
regulatory regions. 354

Motifs download, assignment to target genes, and prior generation 355

We obtained a set of expert-curated motifs for *S. cerevisiae* containing position frequency 356
matrices for yeast transcription factors from The Yeast Transcription Factor Specificity 357
Compendium motifs (YeTFaSCo) [74]. Then, we scanned the whole yeast genome for 358
occurrences of motifs using FIMO with p-value cutoff $1e-4$ [59], and kept motifs that 359
intersected with putative regulatory regions. Each motif was then assigned to the gene 360

with closest downstream transcription start site. Gene annotations were obtained from the 361
Saccharomyces Genome Database (SGD) [75]. A list of putative regulators was downloaded 362
from the YeastMine database [61], and then generated a targets-by-regulators matrix 363
(prior) where entries are the count of motifs for a particular regulator assigned to each gene. 364
Finally, we multiplied entries for repressors by -1. 365

Network inference 366

We approach network inference by modeling gene expression as a weighted sum of the 367
activities of transcription factors [17, 36]. Our goal is to learn these weights from gene 368
expression data as accurately as possible. In this section, we explain our core model of gene 369
regulation, and of transcription factor activities, and state our assumptions. We also 370
describe how we extend our framework to support learning of multiple networks 371
simultaneously, and integration of prior knowledge on network structure. Finally, we 372
explain how we rank predicted interactions which is used to evaluate the ability of these 373
methods to recover the known underlying network. 374

Core model 375

We model the expression of a gene i at condition j , $X_{i,j}$, as the weighted sum of the 376
activities of each transcription factor k at condition j , $A_{k,j}$ [17, 43]. Note that although 377
several methods use transcription factor expression as an approximation for its activity, we 378
explicitly estimate these values from expression data and a set of a prior known interactions. 379
Strength and direction (activation or repression) of a regulatory interaction between 380
transcription factor k and gene i is represented by $w_{i,k}$. At steady state, we assume: 381

$$X_{i,j} = \sum_{k \in TFs} w_{i,k} \hat{A}_{k,j} \quad (1)$$

For time-series, we reason that there is a delay τ between transcription factor activities and 382
resulting changes in target gene expression [43]. Given expression of a gene i in time t_n , 383
 X_{i,t_n} , and activity of transcription factor k at time $t_{n-\tau}$, $A_{k,t_{n-\tau}}$, we assume: 384

$$X_{i,t_n} = \sum_{k \in TFs} w_{i,k} \hat{A}_{k,t_{n-\tau}} \quad (2)$$

If time $t_n - \tau$ is not available in the expression data, linear interpolation is used to fit 385
 $A_{k,t_{n-\tau}}$. 386

Finally, because we expect each gene to be regulated by only a few transcription factors, 387
we seek a sparse solution for w . That is, a solution in which most entries in w are zero. 388

Estimating transcription factor activities (TFA) 389

We use the expression of known targets of a transcription factor to estimate its activity. 390
From a set of prior interactions, we build a connectivity matrix P , where entries represent 391
known activation, $P_{i,k} = 1$, or repression, $P_{i,k} = -1$, of gene i by transcription factor k . If 392
no known interaction, $P_{i,k} = 0$. We assume that the expression of a gene can be written as 393
a linear combination of the activities of its prior known regulators [17]. 394

$$X_{i,j} = \sum_{p \in TFs} P_{i,p} A_{p,j} \quad (3)$$

In case of time-series experiments, we use the expression of genes at time $t_{n+\tau/2}$, $X_{i,t_{n+\tau/2}}$, 395
to inform the activities at time t_n , A_n . Note that for estimating activities, the time delay 396
used is $\tau/2$. Again, linear interpolation is used to estimate $X_{i,t_{n+\tau/2}}$ if gene expression at 397
 $t_{n+\tau/2}$ was not measured experimentally [17]. 398

$$X_{i,t_{n+\tau/2}} = \sum_{p \in TFs} P_{i,p} A_{p,t_n} \quad (4)$$

In matrix form, both time-series and steady-state equations can be written as $X = PA$. 399

Since there are more target genes than regulators $i > p$, this is an over-determined system, 400

and thus has no solution, we approximate A by finding \hat{A} that minimizes $\|P\hat{A} - X\|_2^2$. The 401

solution is given by $\hat{A} = P^*X$, where $P^* = (P^T P)^{-1} P^T$, the pseudo-inverse of P . Finally, 402

for transcription factors with no targets in P , we use the measured expression values as 403

proxy for the activities. 404

Learning regression parameters 405

Given gene expression and activity estimates, the next step is to define a set of regulatory 406

hypotheses for the observed changes in gene expression. For each gene, we find a sparse 407

solution for the regression coefficients where nonzero values indicate the transcription 408

factors that better explain the changes observed in gene expression. In this section, we 409

explain how we learn these parameters from a single dataset (single-task learning) and 410

from multiple (multitask learning). 411

Single-task learning using lasso regression (l_1) 412

The lasso (least absolute selection and shrinkage operator) is a method that performs both 413

shrinkage of the regression coefficients and model selection [49]. That is, it shrinks 414

regression coefficients towards zero, while setting some of them to exactly zero. It does so 415

by adding a penalty on the sum of the absolute values of the estimated regression 416

coefficients. Let \hat{A} be the activities matrix, X_i the expression values for gene i , and w the 417

vector of coefficients, lasso estimates are given by: 418

$$\arg \min_w \frac{1}{2n} \|X_i - \hat{A}^T w\|_2^2 + \lambda \|w\|_1 \quad (5)$$

Where $\|w\|_1 = \sum_k |w_k|$. When minimizing the above function, we seek a good fit while 419

subject to a “budget” on the regression coefficients. The hyper-parameter λ controls how 420

much weight to put on the l_1 penalty. The lasso became very popular in the last decade, 421
because it reduces overfitting and automatically performs variable selection. We choose the 422
lasso as a single-task baseline because it is equivalent to the S matrix in the multitask case 423
(see below), but with independent choice of sparsity parameter for each dataset. 424

Multitask learning using sparse block-sparse regression ($l_1/l_1 + l_1/l_\infty$) 425

We extend our core model to the multiple linear regression setting to enable simultaneous 426
parameter estimation. Here we represent regression parameters for a single gene i as a 427
matrix W , where rows are transcription factors k and columns are networks (or datasets) d . 428
We seek to learn the support $Supp(W)$, where nonzero entries $W_{k,d}$ represent a regulatory 429
interaction between transcription factor k and gene i for network from dataset d . 430

$$X_{i,j}^{(d)} = \sum_{k \in TFS} W_{k,d} \hat{A}_{k,j}^{(d)} \quad (6)$$

For a given gene i , we could assume that the same regulatory network underlies the 431
expression data in all datasets d . That is, rows in W are either completely non-zero or zero. 432
Since a different set of experiments may have different regulatory patterns, this could be a 433
very strong assumption. A more realistic scenario would be that for each gene i , certain 434
regulators are relevant to regulatory models for all datasets d , while others may be selected 435
independently by each model d . Thus, some rows in the parameter matrix W are entirely 436
nonzero or zero, while others do not follow any particular rule. In this scenario, the main 437
challenge is that a single structural constraint such as row-sparsity does not capture the 438
structure of the parameter matrix W . For these problems, a solution is to model the 439
parameter matrix as the combination of structurally constrained parameters [76]. 440

As proposed by Jalali et al. [32], we learn the regression coefficients by decomposing W 441
into B and S , that encode similarities and differences between regulatory models 442
respectively. This representation combines a block-regularization penalty on B enforcing 443

row-sparsity $\|B\|_{1,\infty} = \sum_k \|B_k\|_\infty$, where $\|B_k\|_\infty := \max_d |B_{k,d}|$ (as the one from the 444
 previous section), and an elementwise penalty on S allowing for deviation across regulatory 445
 models for each dataset $\|S\|_{1,1} = \sum_{k,d} |S_{k,d}|$. The goal is to leverage any parameter 446
 overlap between models through B , while accommodating the differences through S . We 447
 obtain an estimate for \hat{W} by solving the following optimization problem: 448

$$\arg \min_{S,B} \frac{1}{2n} \sum_d \|X_i^{(d)} - \hat{A}^{(d)T}(S_{*,d} + B_{*,d})\|_2^2 + \lambda_s \|S\|_{1,1} + \lambda_b \|B\|_{1,\infty} \quad (7)$$

$$\text{output : } \hat{W} = \hat{B} + \hat{S} \quad 449$$

Incorporating prior knowledge using the adaptive lasso 450

We incorporate prior knowledge by differential shrinkage of regression parameters in S 451
 through the adaptive lasso [33]. We choose to apply this only to the S component, because 452
 we wanted to allow the user to input different priors for each dataset if so desired. 453
 Intuitively, we penalize less interactions present in the prior network. Let Φ be a matrix of 454
 regulators k by datasets d , such that entries $\Phi_{k,d}$ are inversely proportional to our prior 455
 confidence on the interaction between regulator k and gene i for dataset d . We then 456
 optimize the following objective: 457

$$\arg \min_{S,B} \frac{1}{2n} \sum_d \|X_i^{(d)} - \hat{A}^{(d)T}(S_{*,d} + B_{*,d})\|_2^2 + \lambda_s \sum_{k,d} |\Phi_{k,d} S_{k,d}| + \lambda_b \|B\|_{1,\infty} \quad (8)$$

$$\text{output : } \hat{W} = \hat{B} + \hat{S} \quad 458$$

We implement this by scaling λ_s by Φ , then the penalty applied to $S_{k,d}$ becomes $\Phi_{k,d} \lambda_s$. In 459
 the extreme $\Phi_{k,d} = 0$, the regulator k is not penalized and will be necessarily included in 460
 the final model for dataset d . In practice, the algorithm accepts an input prior weight 461
 $\rho \geq 1$ that is used to generate the matrix Φ . We apply the complexity-penalty reduction 462

afforded by $\Phi_{k,d}$ to \hat{S} and not \hat{B} as this choice penalizes unique terms, creating the correct 463
behavior of encouraging model differences that are in accord with orthogonal data as 464
expressed in the network-prior. This choice is also in accord with the interpretation of the 465
prior as valid in one, but not necessarily all, conditions. If regulator k is in the prior for 466
dataset d , then $\Phi_{k,d} = 1/\rho$, otherwise $\Phi_{k,d} = 1$. Finally, we rescale $\Phi_{*,d}$ to sum to the 467
number of predictors k . Note that each network model accepts its own set of priors. 468

Model selection 469

As proposed by Jalali et al. [32], for MTL, we set $\lambda_b = c\sqrt{\frac{d \log p}{n}}$, with n being the number 470
of samples, d being the number of datasets, and search for c in the logarithmic interval 471
[0.01, 10]. For each λ_b , we look for λ_s that satisfy $\frac{1}{2} < \frac{\lambda_s}{\lambda_b} < 1$. We choose the optimal 472
combination (λ_s, λ_b) that minimizes the extended Bayesian information criterion 473
(EBIC) [77], here defined as: 474

$$EBIC = \frac{1}{d} \sum_d n_d \ln \frac{1}{n_d} \|X_i^{(d)} - \hat{A}^{(d)T} W_{*,d}\|_2^2 + 2k_d \ln n_d + 2\gamma \ln \binom{p_d}{k_d} \quad (9)$$

with k_d being the number of nonzero predictors in W for model d , and $0 < \gamma < 1$. Note 475
that for $\gamma = 0$, we recover the original BIC. Whereas for $\gamma > 0$, the EBIC scales with the 476
predictor space k making it particularly appropriate for scenarios where $p \gg n$, often 477
encountered in biological network inference projects. In this study, we set $\gamma = 1$. For STL, 478
we use the same EBIC measure, but we calculate it for each dataset separately. 479
Importantly, model selection using EBIC is significantly faster than when compared to 480
re-sampling approaches, such as cross-validation or stability selection [78]. Cross-validation, 481
for example, was previously reported as an impediment for multitask learning in large-scale 482
network inference due computational feasibility [29]. 483

Implementation

484

We implemented the MTL objective function using cyclical coordinate descent with
 covariance updates. That is, at each iteration of the algorithm we cycle through the
 predictors (coordinates), and minimize the objective at each predictor k while keeping the
 others fixed. Briefly, for a given (λ_s, λ_b) , we update entries in S and B respectively, while
 keeping other values in these matrices unchanged, for several iterations until convergence.
 First, we update values in S by:

485

486

487

488

489

490

$$\hat{S}_{k,d} = \arg \min_{S_{k,d}} \frac{1}{2} \|R_k^{(d)} - S_{k,d} A_k^{(d)}\|_2^2 + \lambda_s \sum_k |S_{*,d}|, \forall k, d \quad (10)$$

with $R_k^{(d)} = X_i^{(d)} - \sum_{l \neq k} (S_{l,d} + B_{l,d}) A_l^{(d)} - \sum_k B_{k,d} A_{k,d}$, being the partial residual vector.

491

Intuitively, we remove effect of the previous coefficient value for $S_{k,d}$, while keeping $B_{k,d}$
 unchanged and measure how it changes the residuals. This represents a measure of how
 important that feature is to the prediction, and contributes to the decision of whether a
 feature is pushed towards zero or not by the lasso penalty. For $\lambda_s = 0$, we can find the
 least squares update, $\alpha_{k,d} = \langle R_k^{(d)}, A_k^{(d)} \rangle$, and re-write as
 $\alpha_{k,d} = \langle A_k^{(d)}, X_i^{(d)} \rangle - \sum_{l \neq k} (S_{l,d} + B_{l,d}) \langle A_l^{(d)}, A_k^{(d)} \rangle - B_{k,d} \langle A_k^{(d)}, A_k^{(d)} \rangle$. This formulation can
 be optimized much quicker using the covariance updates explained below.

492

493

494

495

496

497

498

Then, we update \hat{B}_k , which represents an entire row in B , by:

499

$$\hat{B}_k = \arg \min_{B_k} \frac{1}{2} \sum_d \|R_k^{(d)} - B_{k,d} A_k^{(d)}\|_2^2 + \lambda_b \|B_k\|_\infty, \forall k \quad (11)$$

with $R^{(d)} = X_i^{(d)} - \sum_{l \neq k} (S_{l,d} + B_{l,d}) A_l^{(d)} - \sum_k S_{k,d} A_k^{(d)}$, being the partial residual vector
 for this case. In this case, we keep the value $S_{k,d}$ unchanged, and set $B_{k,d}$ to zero. Similarly,
 we remove effects from previous $B_{k,d}$ and evaluate how this feature is for the prediction;
 this then contributes to the decision of whether this entire row is sent to zero by the infinity

500

501

502

503

norm penalty. For $\lambda_b = 0$, we can find the least squares update, $\alpha_{k,d} = \langle R^{(d)}, A_k^{(d)} \rangle$, which 504
can be re-written as $\alpha_{k,d} = \langle A_k^{(d)}, X_i^{(d)} \rangle - \sum_{l \neq k} (S_{l,d} + B_{l,d}) \langle A_l^{(d)}, A_k^{(d)} \rangle - S_{k,d} \langle A_k^{(d)}, A_k^{(d)} \rangle$. 505
Finally, we apply soft-thresholding to penalize the least-squares updates. 506

Using these formulations for the updates, we can use the idea of covariance updates [50, 79], 507
where the cross-products $A^T A$ and $A^T X$ are stored in separate matrices and reused at 508
every iteration. Because these cross-products correspond to over 95% of computation time, 509
this trick decreases runtime significantly. To further decrease runtime, we also employ 510
warm starts when searching for optimal penalty values (λ_s, λ_b) [79]. Additionally, since we 511
infer regulators for each gene separately, we can parallelize calculations by gene. 512

Estimating prediction confidence scores 513

For each predicted interaction we compute a confidence score that represents how well a 514
predictor explains the expression data, and a measure of prediction stability. As previously 515
proposed [17, 43], we calculate confidence scores for each interaction by: 516

$$c_{k,i} = 1 - \frac{\sigma_{full\ model\ for\ x_i}^2}{\sigma_{model\ for\ x_i\ without\ predictor\ k}^2} \quad (12)$$

where σ^2 equals the variance of the residuals for the models, with and without predictor k . 517
The score $c_{k,i}$ is proportional to how much removing regulator k from gene i set of 518
predictors decreases model fit. To measure stability, we perform the inference across 519
multiple bootstraps of the expression data (we used 20 bootstraps for both *B. subtilis* and 520
yeast), rank-average the interactions across all bootstraps [16, 43], and re-scale the ranking 521
between 0 and 1 to output a final ranked list of regulatory hypotheses. 522

References

1. Margolin AA, Nemenman I, Basso K, Wiggins C, Stolovitzky G, Dalla Favera R, et al. ARACNE: an algorithm for the reconstruction of gene regulatory networks in a mammalian cellular context. *BMC bioinformatics*. 2006;7(1):S7.
2. Petralia F, Wang P, Yang J, Tu Z. Integrative random forest for gene regulatory network inference. *Bioinformatics*. 2015;31(12):i197–i205.
3. Bonneau R, Reiss DJ, Shannon P, Facciotti M, Hood L, Baliga NS, et al. The Inferelator: an algorithm for learning parsimonious regulatory networks from systems-biology data sets de novo. *Genome biology*. 2006;7(5):R36.
4. Yosef N, Shalek AK, Gaublomme JT, Jin H, Lee Y, Awasthi A, et al. Dynamic regulatory network controlling TH17 cell differentiation. *Nature*. 2013;496(7446):461.
5. Ciofani M, Madar A, Galan C, Sellars M, Mace K, Pauli F, et al. A validated regulatory network for Th17 cell specification. *Cell*. 2012;151(2):289–303.
6. Rung J, Brazma A. Reuse of public genome-wide gene expression data. *Nature reviews Genetics*. 2013;14(2):89.
7. Koch C, Konieczka J, Delorey T, Lyons A, Socha A, Davis K, et al. Inference and Evolutionary Analysis of Genome-Scale Regulatory Networks in Large Phylogenies. *Cell systems*. 2017;4(5):543–558.
8. Muir P, Li S, Lou S, Wang D, Spakowicz DJ, Salichos L, et al. The real cost of sequencing: scaling computation to keep pace with data generation. *Genome biology*. 2016;17(1):53.
9. Marx V. Biology: The big challenges of big data. *Nature*. 2013;498(7453):255–260.
10. Leek JT, Scharpf RB, Bravo HC, Simcha D, Langmead B, Johnson WE, et al. Tackling the widespread and critical impact of batch effects in high-throughput data. *Nature reviews Genetics*. 2010;11(10).

11. Nayfach S, Pollard KS. Toward accurate and quantitative comparative metagenomics. *Cell*. 2016;166(5):1103–1116.
12. Pritchard CC, Cheng HH, Tewari M. MicroRNA profiling: approaches and considerations. *Nature reviews Genetics*. 2012;13(5):358.
13. Tung PY, Blischak JD, Hsiao CJ, Knowles DA, Burnett JE, Pritchard JK, et al. Batch effects and the effective design of single-cell gene expression studies. *Scientific reports*. 2017;7:39921.
14. Auer PL, Doerge R. Statistical design and analysis of RNA sequencing data. *Genetics*. 2010;185(2):405–416.
15. Nygaard V, Rødland EA, Hovig E. Methods that remove batch effects while retaining group differences may lead to exaggerated confidence in downstream analyses. *Biostatistics*. 2016;17(1):29–39.
16. Marbach D, Costello JC, Küffner R, Vega NM, Prill RJ, Camacho DM, et al. Wisdom of crowds for robust gene network inference. *Nature Methods*. 2012;9(8):796–804.
17. Arrieta-Ortiz ML, Hafemeister C, Bate AR, Chu T, Greenfield A, Shuster B, et al. An experimentally supported model of the *Bacillus subtilis* global transcriptional regulatory network. *Molecular Systems Biology*. 2015;11(11):839.
18. Dietterich TG, et al. Ensemble methods in machine learning. *Multiple classifier systems*. 2000;1857:1–15.
19. Papp B, Oliver S. Genome-wide analysis of the context-dependence of regulatory networks. *Genome biology*. 2005;6(2):206.
20. Harbison CT, Gordon DB, Lee TI, Rinaldi NJ, Macisaac KD, Danford TW, et al. Transcriptional regulatory code of a eukaryotic genome. *Nature*. 2004;431(7004):99–104.

21. Siahpirani AF, Roy S. A prior-based integrative framework for functional transcriptional regulatory network inference. *Nucleic acids research*. 2017;45(4):e21–e21.
22. Buenrostro JD, Giresi PG, Zaba LC, Chang HY, Greenleaf WJ. Transposition of native chromatin for fast and sensitive epigenomic profiling of open chromatin, DNA-binding proteins and nucleosome position. *Nature methods*. 2013;10(12):1213.
23. Boyle AP, Davis S, Shulha HP, Meltzer P, Margulies EH, Weng Z, et al. High-resolution mapping and characterization of open chromatin across the genome. *Cell*. 2008;132(2):311–322.
24. Johnson DS, Mortazavi A, Myers RM, Wold B. Genome-wide mapping of in vivo protein-DNA interactions. *Science*. 2007;316(5830):1497–1502.
25. Lam KY, Westrick ZM, Müller CL, Christiaen L, Bonneau R. Fused regression for multi-source gene regulatory network inference. *PLoS computational biology*. 2016;12(12):e1005157.
26. Omranian N, Eloundou-Mbebi JM, Mueller-Roeber B, Nikoloski Z. Gene regulatory network inference using fused LASSO on multiple data sets. *Scientific reports*. 2016;6:20533.
27. Jain S, Gitter A, Bar-Joseph Z. Multitask learning of signaling and regulatory networks with application to studying human response to flu. *PLoS computational biology*. 2014;10(12):e1003943.
28. Wang Y, Joshi T, Zhang XS, Xu D, Chen L. Inferring gene regulatory networks from multiple microarray datasets. *Bioinformatics*. 2006;22(19):2413–2420.
29. Chasman D, Walters KB, Lopes TJ, Eisfeld AJ, Kawaoka Y, Roy S. Integrating Transcriptomic and Proteomic Data Using Predictive Regulatory Network Models of Host Response to Pathogens. *PLoS computational biology*. 2016;12(7):e1005013.

30. Gupta R, Stincone A, Antczak P, Durant S, Bicknell R, Bikfalvi A, et al. A computational framework for gene regulatory network inference that combines multiple methods and datasets. *BMC systems biology*. 2011;5(1):52.
31. Qin J, Hu Y, Xu F, Yalamanchili HK, Wang J. Inferring gene regulatory networks by integrating ChIP-seq/chip and transcriptome data via LASSO-type regularization methods. *Methods*. 2014;67(3):294–303.
32. Jalali A, Sanghavi S, Ruan C, Ravikumar PK. A dirty model for multi-task learning. In: *Advances in Neural Information Processing Systems*; 2010. p. 964–972.
33. Zou H. The adaptive lasso and its oracle properties. *Journal of the American statistical association*. 2006;101(476):1418–1429.
34. Caruana R. Multitask learning. In: *Learning to learn*. Springer; 1998. p. 95–133.
35. Chen X, Xuan J, Wang C, Shajahan AN, Riggins RB, Clarke R. Reconstruction of transcriptional regulatory networks by stability-based network component analysis. *IEEE/ACM transactions on computational biology and bioinformatics*. 2013;10(6):1347–1358.
36. Fu Y, Jarboe LR, Dickerson JA. Reconstructing genome-wide regulatory network of *E. coli* using transcriptome data and predicted transcription factor activities. *BMC bioinformatics*. 2011;12(1):233.
37. Dai Z, Iqbal M, Lawrence ND, Rattray M. Efficient inference for sparse latent variable models of transcriptional regulation. *Bioinformatics*. 2017;33(23):3776–3783.
38. Liao JC, Boscolo R, Yang YL, Tran LM, Sabatti C, Roychowdhury VP. Network component analysis: reconstruction of regulatory signals in biological systems. *Proceedings of the National Academy of Sciences*. 2003;100(26):15522–15527.
39. Sanguinetti G, Lawrence ND, Rattray M. Probabilistic inference of transcription factor concentrations and gene-specific regulatory activities. *Bioinformatics*. 2006;22(22):2775–2781.

40. Filtz TM, Vogel WK, Leid M. Regulation of transcription factor activity by interconnected post-translational modifications. *Trends in pharmacological sciences*. 2014;35(2):76–85.
41. Ravasi T, Suzuki H, Cannistraci CV, Katayama S, Bajic VB, Tan K, et al. An atlas of combinatorial transcriptional regulation in mouse and man. *Cell*. 2010;140(5):744–752.
42. Shlyueva D, Stampfel G, Stark A. Transcriptional enhancers: from properties to genome-wide predictions. *Nature Reviews Genetics*. 2014;15(4):272–286.
43. Greenfield A, Hafemeister C, Bonneau R. Robust data-driven incorporation of prior knowledge into the inference of dynamic regulatory networks. *Bioinformatics*. 2013;29:1060–1067.
44. Han H, Shim H, Shin D, Shim JE, Ko Y, Shin J, et al. TRRUST: a reference database of human transcriptional regulatory interactions. *Scientific reports*. 2015;5:11432.
45. Gama-Castro S, Salgado H, Peralta-Gil M, Santos-Zavaleta A, Muniz-Rascado L, Solano-Lira H, et al. RegulonDB version 7.0: transcriptional regulation of *Escherichia coli* K-12 integrated within genetic sensory response units (Gensor Units). *Nucleic acids research*. 2010;39(suppl_1):D98–D105.
46. Michna RH, Zhu B, Mäder U, Stülke J. Subti Wiki 2.0—an integrated database for the model organism *Bacillus subtilis*. *Nucleic acids research*. 2015;44(D1):D654–D662.
47. Teixeira MC, Monteiro P, Jain P, Tenreiro S, Fernandes AR, Mira NP, et al. The YEASTRACT database: a tool for the analysis of transcription regulatory associations in *Saccharomyces cerevisiae*. *Nucleic acids research*. 2006;34(suppl_1):D446–D451.

48. Arnone MI, Davidson EH. The hardwiring of development: organization and function of genomic regulatory systems. *Development*. 1997;124(10):1851–1864.
49. Tibshirani R. Regression shrinkage and selection via the lasso. *Journal of the Royal Statistical Society Series B (Methodological)*. 1996; p. 267–288.
50. Liu H, Palatucci M, Zhang J. Blockwise coordinate descent procedures for the multi-task lasso, with applications to neural semantic basis discovery. In: *Proceedings of the 26th Annual International Conference on Machine Learning*. ACM; 2009. p. 649–656.
51. Tchourine K, Vogel C, Bonneau R. Explicit Modeling of RNA Stability Improves Large-Scale Inference of Transcription Regulation. *bioRxiv*. 2017;doi:10.1101/104885.
52. Nicolas P, Mäder U, Dervyn E, Rochat T, Leduc A, Pigeonneau N, et al. Condition-dependent transcriptome reveals high-level regulatory architecture in *Bacillus subtilis*. *Science*. 2012;335(6072):1103–1106.
53. Hibbs MA, Hess DC, Myers CL, Huttenhower C, Li K, Troyanskaya OG. Exploring the functional landscape of gene expression: directed search of large microarray compendia. *Bioinformatics*. 2007;23(20):2692–2699.
54. Knijnenburg TA, Daran JMG, van den Broek MA, Daran-Lapujade PA, de Winde JH, Pronk JT, et al. Combinatorial effects of environmental parameters on transcriptional regulation in *Saccharomyces cerevisiae*: a quantitative analysis of a compendium of chemostat-based transcriptome data. *BMC genomics*. 2009;10(1):53.
55. Smith EN, Kruglyak L. Gene–environment interaction in yeast gene expression. *PLoS biology*. 2008;6(4):e83.
56. Hughes TR, Marton MJ, Jones AR, Roberts CJ, Stoughton R, Armour CD, et al. Functional discovery via a compendium of expression profiles. *Cell*. 2000;102(1):109–126.

57. Costanzo MC, Engel SR, Wong ED, Lloyd P, Karra K, Chan ET, et al. Saccharomyces genome database provides new regulation data. *Nucleic acids research*. 2013;42(D1):D717–D725.
58. Weirauch MT, Yang A, Albu M, Cote AG, Montenegro-Montero A, Drewe P, et al. Determination and inference of eukaryotic transcription factor sequence specificity. *Cell*. 2014;158(6):1431–1443.
59. Grant CE, Bailey TL, Noble WS. FIMO: scanning for occurrences of a given motif. *Bioinformatics*. 2011;27(7):1017–1018.
60. Karwacz K, Miraldi ER, Pokrovskii M, Madi A, Yosef N, Wortman I, et al. Critical role of IRF1 and BATF in forming chromatin landscape during type 1 regulatory cell differentiation. *Nature immunology*. 2017;18(4):412.
61. Balakrishnan R, Park J, Karra K, Hitz BC, Binkley G, Hong EL, et al. YeastMine—an integrated data warehouse for *Saccharomyces cerevisiae* data as a multipurpose tool-kit. *Database*. 2012;2012.
62. Tsompana M, Buck MJ. Chromatin accessibility: a window into the genome. *Epigenetics & chromatin*. 2014;7(1):33.
63. Kittler J, Hatef M, Duin RP, Matas J. On combining classifiers. *IEEE transactions on pattern analysis and machine intelligence*. 1998;20(3):226–239.
64. Johnson WE, Li C, Rabinovic A. Adjusting batch effects in microarray expression data using empirical Bayes methods. *Biostatistics*. 2007;8(1):118–127.
65. Müller C, Schillert A, Röthemeier C, Trégouët DA, Proust C, Binder H, et al. Removing Batch Effects from Longitudinal Gene Expression-Quantile Normalization Plus ComBat as Best Approach for Microarray Transcriptome Data. *PloS one*. 2016;11(6):e0156594.
66. MacNeil LT, Walhout AJ. Gene regulatory networks and the role of robustness and stochasticity in the control of gene expression. *Genome research*. 2011;21(5):645–657.

67. Gitter A, Siegfried Z, Klutstein M, Fornes O, Oliva B, Simon I, et al. Backup in gene regulatory networks explains differences between binding and knockout results. *Molecular systems biology*. 2009;5(1):276.
68. Hecker M, Lambeck S, Toepfer S, Van Someren E, Guthke R. Gene regulatory network inference: data integration in dynamic models—a review. *Biosystems*. 2009;96(1):86–103.
69. Waltman P, Kacmarczyk T, Bate AR, Kearns DB, Reiss DJ, Eichenberger P, et al. Multi-species integrative biclustering. *Genome biology*. 2010;11(9):R96.
70. Schep AN, Buenrostro JD, Denny SK, Schwartz K, Sherlock G, Greenleaf WJ. Structured nucleosome fingerprints enable high-resolution mapping of chromatin architecture within regulatory regions. *Genome research*. 2015;25(11):1757–1770.
71. Leinonen R, Akhtar R, Birney E, Bower L, Cerdeno-Tárraga A, Cheng Y, et al. The European nucleotide archive. *Nucleic acids research*. 2010;39(suppl_1):D28–D31.
72. Langmead B, Salzberg SL. Fast gapped-read alignment with Bowtie 2. *Nature methods*. 2012;9(4):357–359.
73. Zhang Y, Liu T, Meyer CA, Eeckhoutte J, Johnson DS, Bernstein BE, et al. Model-based analysis of ChIP-Seq (MACS). *Genome biology*. 2008;9(9):R137.
74. de Boer CG, Hughes TR. YeTFaSCo: a database of evaluated yeast transcription factor sequence specificities. *Nucleic acids research*. 2011;40(D1):D169–D179.
75. Cherry JM. The *Saccharomyces* Genome Database: A Tool for Discovery. *Cold Spring Harbor Protocols*. 2015;2015(12):pdb-top083840.
76. Yang E, Ravikumar PK. Dirty statistical models. In: *Advances in Neural Information Processing Systems*; 2013. p. 611–619.
77. Chen J, Chen Z. Extended Bayesian information criteria for model selection with large model spaces. *Biometrika*. 2008;95(3):759–771.

78. Meinshausen N, Bühlmann P. Stability selection. *Journal of the Royal Statistical Society: Series B (Statistical Methodology)*. 2010;72(4):417–473.
79. Friedman J, Hastie T, Tibshirani R. Regularization paths for generalized linear models via coordinate descent. *Journal of statistical software*. 2010;33(1):1.

Figure Legends

Fig 1: Gene regulatory network inference schematic. (A) Our network inference algorithm takes as input a gene expression matrix, X , and a prior on network structure and outputs regulatory hypotheses of regulator-target interactions. (B) Using priors on network topology and gene expression data, we estimate transcription factor activities (TFA), and subsequently model gene expression as a function of these activities. (C) We use several possible sources of prior information on network topology. (D) Prior information is encoded in a matrix P , where positive and negative entries represent known activation and repression respectively, whereas zeros represent absence of known regulatory interaction. To estimate hidden activities, we consider $X = PA$ (top), where the only unknown is the activities. Of note, a time-delay is implemented for time-series experiments (bottom). (E) Finally, for each gene, we find regulators that influence its expression using regularized linear regression. We either learn these influences, or weights, for each dataset independently, single-task learning (top), or jointly through multi-task learning (bottom).

Fig 2: Representation of the weights matrix for one gene in the multitask setting. We represent model coefficients as a matrix W (predictors by datasets) where nonzero rows represent predictors relevant for all datasets. We decompose the weights into two components, and regularize them differently, using a sparse penalty (l_1/l_1 to S component) to encode a dataset-specific component and a block-sparse penalty (l_1/l_∞ to B component) to encode a conserved one. To illustrate, in this example, non-zero weights are shown on the right side. Note that, in this schematic example, regulators w_3 and w_7 are shared between all datasets. We also show (bottom) the objective function minimized to estimate S and B on the bottom (for details, see methods).

Fig 3: Multitask learning increase confidence scores of interactions in the gold-standard, improving accuracy of inferred networks. (A) Relationship

between TF activity and target expression in *B. subtilis* 1 (blue) and in *B. subtilis* 2 (orange), and corresponding STL and MTL inferred confidence scores for an example of an interaction in the *B. subtilis* gold-standard, sigD to lytA. (B) as shown in (A), but for an interaction in the *S. cerevisiae* gold-standard, Msn2 to Hsp104. (C) Inferred confidence scores for interactions in the gold-standard for all datasets. In each plot, dots on the left show scores learned through STL, whereas dots on the right are scores learned through MTL. Lines connect scores associated with the same interaction. (D) Precision-recall curves assessing accuracy of network models inferred for individual *B. subtilis* datasets against a leave-out set of interactions. For simplicity, only one replicate is shown in the curve. Barplot with mean area under precision-recall curve (AUPR) for each method and dataset. Error bars show the standard deviation across 10 splits of the gold-standard into prior and evaluation set. (E) Precision-recall curves assessing accuracy of network models inferred for individual *S. cerevisiae* networks, with the difference that the prior is from an independent source (no splits or replicates).

Fig 4: Multitask learning performance boost outweighs benefits of other data integration methods. Assessment of accuracy of network models learned using three different data integration strategies, data merging and batch correction (STL-BC), ensemble method combining models learned independently (STL-C), and ensemble method combining models learned jointly (MTL-C). (A) Precision-recall curves for *B. subtilis*, again using a leave-out set of interactions. For simplicity, only one replicate is shown in the curve. Barplot with mean area under precision-recall curve (AUPR) for each method. Error bars show the standard deviation across 10 splits of the gold-standard into prior and evaluation set. (B) Precision-recall curves for *S. cerevisiae*, with the difference that the prior is from an independent source (no splits or replicates).

Fig 5: Recovery of prior interactions depends on prior quality and is robust to increasing prior weights. Distribution of number of regulators per target in the *B.*

subtilis prior (A), for the *S. cerevisiae* gold-standard (B), and for the *S. cerevisiae* chromatin accessibility-derived priors (C). (D) Distributions of MTL inferred confidence scores for interactions in the prior for each dataset. Different colors show prior weights used, and represent an amount by which interactions in the prior are favored by model selection when compared to interactions without prior information.

Fig 6: Overlap of edges in inferred networks is higher for *B. subtilis* than for *S. cerevisiae*. Edges overlap across networks inferred using multitask learning for *B. subtilis* (prior weight of 1.0) (A), for *S. cerevisiae* (using the gold-standard as priors) (B), for *S. cerevisiae* (using the chromatin accessibility-derived priors) (C).

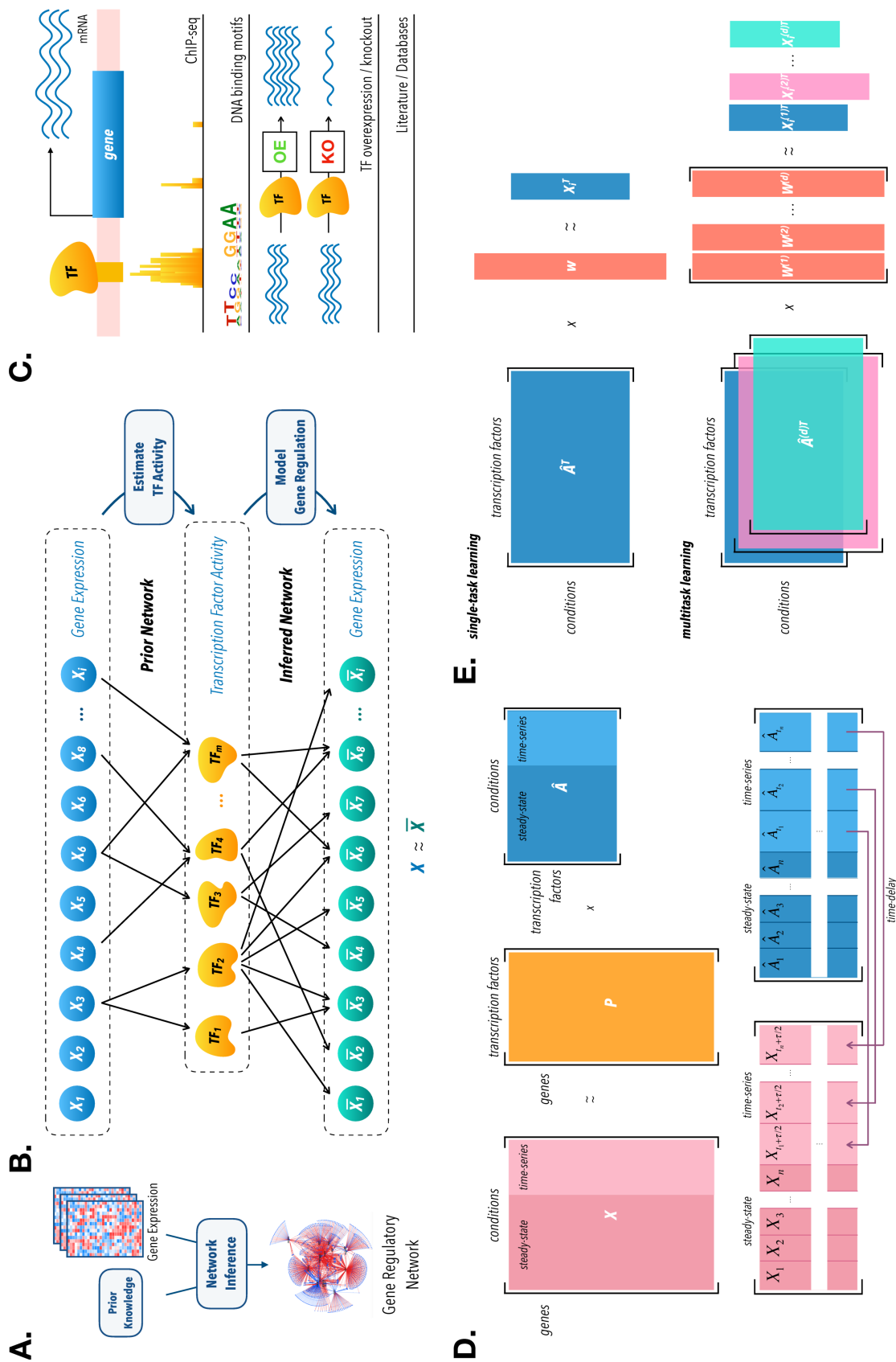
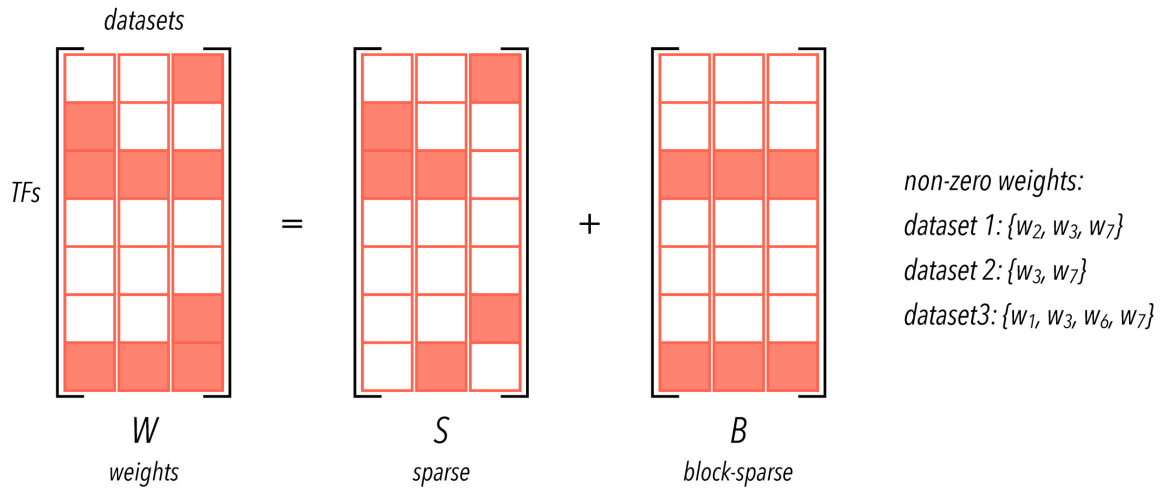


Fig 1. Gene regulatory network inference schematic



$$\arg \min_{S, B} \frac{1}{2n} \sum_d \|X_i^{(d)} - \hat{A}^{(d)T}(S_{*,d} + B_{*,d})\|_2^2 + \lambda_s \sum_{k,d} |\Phi_{k,d} S_{k,d}| + \lambda_b \|B\|_{1,\infty}$$

$$\text{output} : \hat{W} = \hat{B} + \hat{S}$$

Fig 2. Representation of the weights matrix for one gene in the multitask setting.

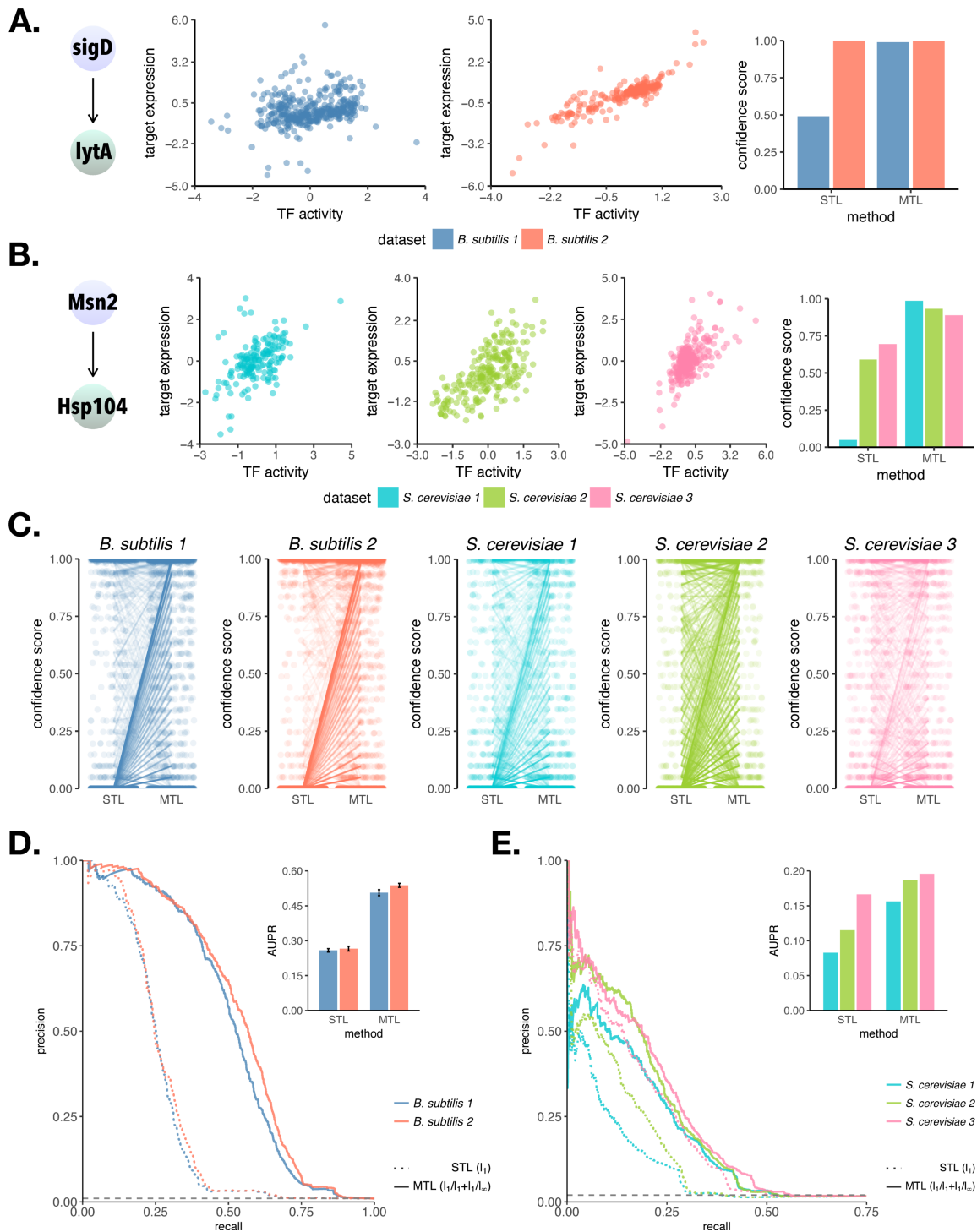


Fig 3. Multitask learning Increase Confidence Scores of Interactions in the Gold-Standard, thus Improving Accuracy of Inferred Networks

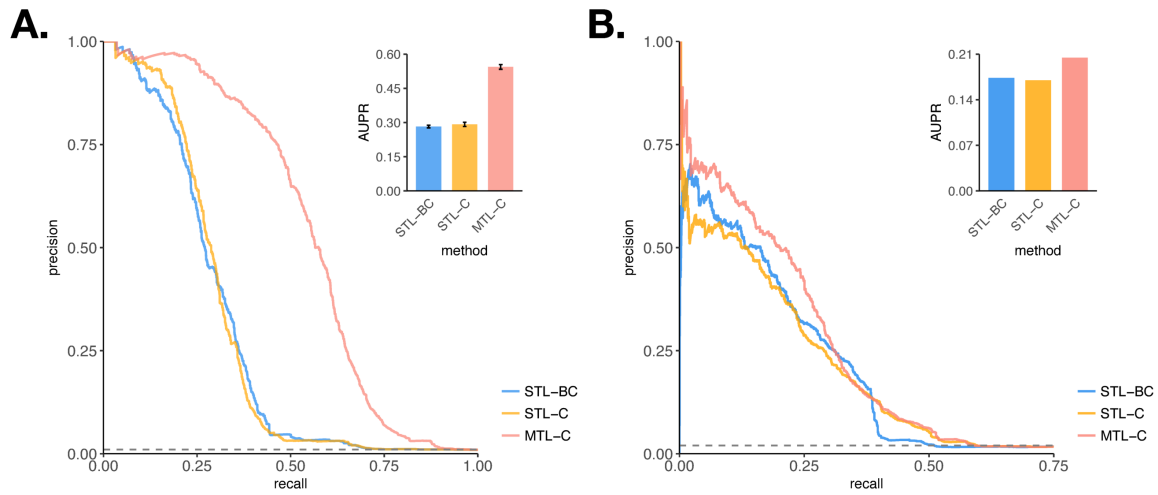


Fig 4. Multitask Learning Boost in Performance Outweighs Benefits of Other Data Integration Methods

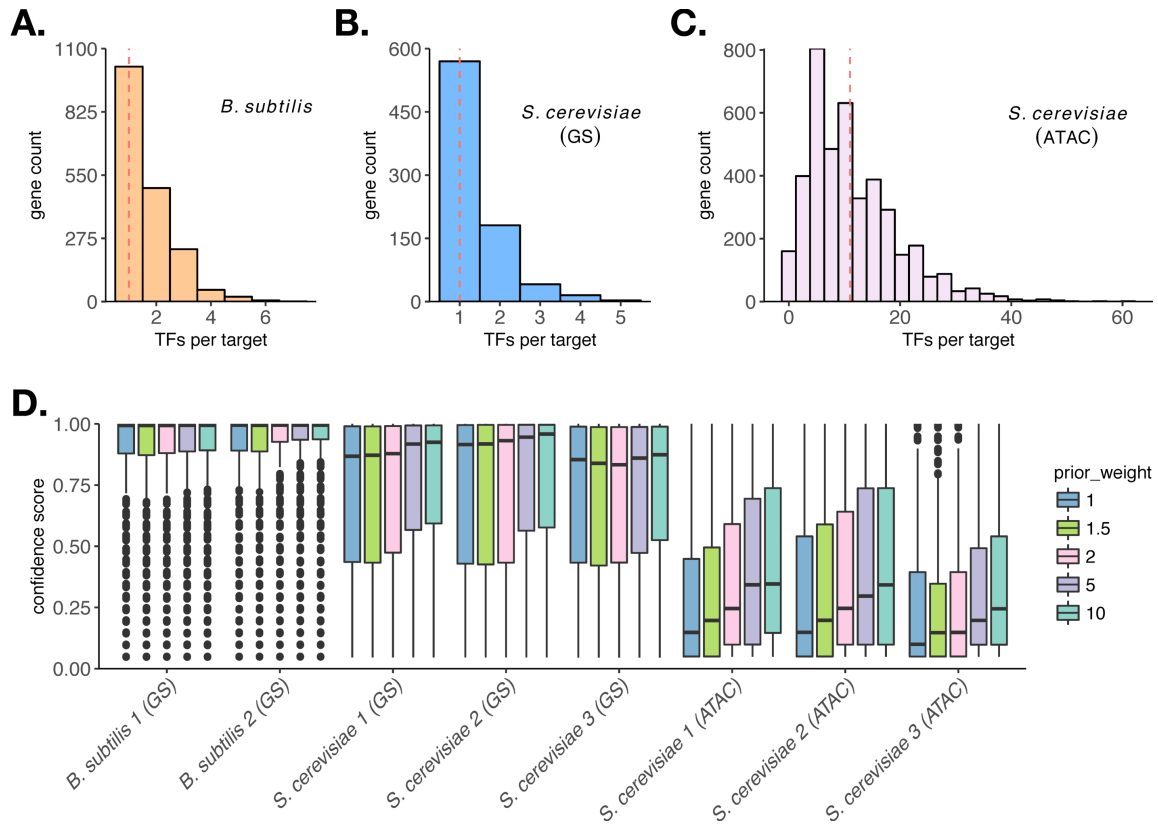


Fig 5. Recovery of Prior Interactions Depends on Prior Quality and is Robust to Increasing Prior Weights

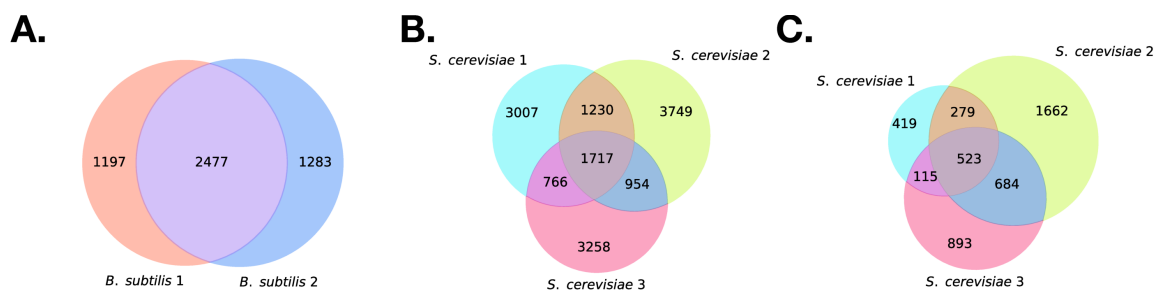


Fig 6. Cross-dataset overlap of inferred edges is higher for *B. subtilis* than for *S. cerevisiae*